High-resolution polypeptide structure in a lamellar phase lipid environment from solid state NMR derived orientational constraints

RR Ketchem[1†], B Roux[2] and TA Cross[1*]

Background: Solid-state nuclear magnetic resonance (NMR) spectroscopy provides novel structural constraints from uniformly aligned samples. These orientational constraints orient specific atomic sites with respect to the magnetic field direction and the unique molecular axis of alignment. Solid-state NMR is uniquely and ideally suited for providing such structural constraints on polypeptides and proteins in a lamellar phase lipid environment. Membrane protein structure represents a great challenge for structural biologists; a new approach for characterizing high resolution three-dimensional structure in such an environment is needed.

Results: The optimal use of orientational constraints for defining three-dimensional structures is demonstrated with the elucidation of the gramicidin A channel structure at high resolution. Initial structures are refined against both the experimental constraints and the CHARMM energy using a novel simulated-annealing protocol to define torsion angle solutions with an error bar of approximately ± 5°.

Conclusions: This analysis results in the determination of a high-resolution, time averaged structure of gramicidin A obtained in a lipid bilayer environment above the gel-to-liquid crystalline phase transition temperature. It is demonstrated that solid-state NMR can be used to establish polypeptide, and potentially protein, structures in such an environment. Furthermore, this high-resolution structure is demonstrated to provide new insights into polypeptide function. For the gramicidin A channel the roles of the indole groups that facilitate ion transport and details of the cation solvation environment provided by the amide oxygens are characterized.

Addresses: [1]Center for Interdisciplinary Magnetic Resonance at the National High Magnetic Field Laboratory, Institute of Molecular Biophysics and Department of Chemistry, Florida State University, Tallahassee, FL 32306-4005, USA and [2]Groupe de Recherche en Transport Membranaire, Departments of Physique and Chemistry, Universit'e de Montr'eal, C.P. 6128, succ. Centr-Ville, H3C-3J7 Canada.

[†]Present address: Department of Molecular Biology, MB-9, The Scripps Research Institute, 10550 North Torrey Pines Road, La Jolla, CA 92037-1027, USA.

*Corresponding author.
E-mail: cross@magnet.fsu.edu

Key words: CHARMM energy, gramicidin A, membrane protein structure, orientational constraints, solid-state NMR

Received: **14 August 1997**
Revisions requested: **11 September 1997**
Revisions received: **10 October 1997**
Accepted: **23 October 1997**

Structure 15 December 1997, **5**:1655–1669
http://biomednet.com/elecref/0969212600501655

Introduction

High-resolution structures have the potential to unveil the solutions to many of the functional questions about macromolecules, but the value of the structure is dependent on obtaining experimental data in an environment that closely models the native environment. Membrane proteins and polypeptides have been very difficult to study because cocrystallization of lipids and proteins has been rarely achieved and solution NMR studies are restricted to small molecular weight proteins in model membrane environments with high surface curvature. In this study, the gramicidin A structure in planar lipid bilayers, obtained from solid-state NMR-derived orientational constraints, was refined to high resolution against these experimental constraints and the CHARMM global energy [1]. This experimental data precisely constrained the molecular sites to the laboratory frame of reference. The refinement protocol has the challenge of thoroughly searching only the local conformational space about the viable structural possibilities separated by high penalty barriers.

Gramicidin A is a hydrophobic linear polypeptide of 15 residues with alternating L and D stereochemistry and blocked N and C terminal residues: formyl-Val1-Gly2-Ala3-DLeu4-Ala5-DVal6-Val7-DVal8-Trp9-DLeu10-Trp11-Leu12-Trp13-DLeu14-Trp15-ethanolamine.

In organic solvents, gramicidin forms a variety of well characterized double helical structures. Many crystallography [2–4] and solution NMR studies [5–8] have been performed on these conformers. The single-stranded channel state has been studied by both solution NMR in micellar environments [7,9] and solid-state NMR in lipid bilayer environments [10–16]. While the fold of the peptide is the same in the micelles and bilayers, the sidechain conformations and detailed structural aspects of the backbone are different [17]. There have also been many computational studies that have focused on details of the structure and dynamics as pertaining to cation interactions [18–22], solvent in the channel [23] and the lipid environment [24–25].

Gramicidin A, as a dimer, forms a monovalent cation selective channel that has been the subject of numerous single channel conductance studies [26–28]. This peptide forms narrow pores in lipid bilayers, not unlike selectivity

filters in large proteinaceous channels. These physiology experiments have been extended to a variety of gramicidin A analogs that show changes in conductance and channel lifetimes [29,30] and even voltage-gating of the channel [31]. While important physiological phenomena have been observed for the gramicidin channels, there has been a dearth of structural or dynamic data for explaining these phenomena.

In recent years, structural constraints for macromolecules have been derived from solid-state NMR both in the form of distance and orientational constraints. Two fundamentally different approaches have been used for obtaining distance constraints, REDOR [32,33] and Rotational Resonance [34,35]. Families of different experiments have now been generated based on these methods. In this study we have used orientational constraints measured from samples uniformly aligned with respect to the magnetic field direction. Each of these constraints orients the molecular frame of an atomic site with respect to the magnetic field and a unique molecular axis. In this study this molecular axis is both the lipid bilayer normal and the channel axis, both of which are aligned parallel to the magnetic field direction. The orientational constraints are derived from the orientation dependence of nuclear spin interactions; for the gramicidin monomer, 120 uniquely assigned constraints have been obtained using a variety of spin interactions. Each of these interactions is described in the molecular frame by a tensor or coordinate system.

The initial analysis of these constraints to generate a family of molecular structures has been accomplished [16,36]. Briefly, each peptide linkage is considered a plane and its orientation is defined by two dipolar interactions, ^{15}N–^{1}H and ^{15}N–$^{13}C_1$. The unique axis of these spin interaction tensors is parallel to the internuclear vector, that is the N–H and N–C_1 bonds. The orientation of each plane is thereby defined with respect to the magnetic field direction, but the cosine of the normal to this plane has an undefined sign. This ambiguity has recently been described as a chirality [37]. Those peptide planes in which the C–O vector is rotated slightly in towards the channel axis are defined as '+' and those with the C–O vector oriented away from the channel axis are defined as '–'. Any combination of chirality solutions yields the same folding motif for this structure as shown by Ketchem *et al.*, [36]. Other backbone structural ambiguities have previously been resolved through the use of orientational constraints derived from anisotropic $^{15}N_\alpha$ chemical shifts and C_α–^{2}H quadrupolar interactions [36,38].

Sidechains of the gramicidin A aliphatic amino acids have been structurally and dynamically characterized by ^{2}H NMR. Because of rapid methyl group dynamics, the C_{Me}–H bond orientations are motionally averaged and only the C–C_{Me} axis orientation is characterized for the methyl groups. The only large amplitude dynamics in these sidechains occurs with the Val1 and Val7 sidechains which are dominated by a single rotameric state, although all three χ_1 rotamers are populated [39]. These independent determinations of rotamer populations have been achieved with temperature-dependent powder pattern analysis. For the initial structures used here the Val1 and Val7 sidechains were placed in their dominant χ_1 state. For the Val6 and Val8 sidechains unique rotameric states have been defined [39]. The leucine sidechains show no large amplitude dynamics and unique χ_1 values are defined for each residue [36]. In addition, unique χ_2 values are defined for Leu12 and Leu14. Most probable values (based on torsional energy) for Leu4 and Leu10, from two possible χ_2 values for each, have been chosen. From ^{2}H and ^{15}N spectroscopy of the indole sidechains, four χ_1, χ_2 solution pairs have been defined based on the orientational constraints alone [40]. Compelling functional data and energetic arguments, however, have led to a most probable solution for each indole [41] and just recently data obtained from Raman spectroscopy has argued strongly against two of the four possible solutions for each of the indoles [42].

As the fundamental repeating structural unit in this β-sheet type structure is a dipeptide, chirality patterns for adjacent peptide planes of +/+, +/–, –/+ and –/– encompass the range of backbone conformations shown in Figure 1. The differences between these initial backbone structures is illustrated with the distance difference matrix (DDM) [43,44] plots in Figure 2. These plots represent the difference between two matrices of backbone interatomic distances using the N, H_N, C_α, C_1 and O atoms. A matrix of intramolecular distances is defined for each structure and the comparison of two structures is achieved by subtracting one matrix from another without having to superimpose structures. While it is clear that there are significant (> 1 Å) differences throughout these structural comparisons, it is also clear that differences are not much greater when comparing residues 1 and 15 versus 1 and 3. In other words the differences are not cumulative. In all of these initial structures there are significant structural imperfections [17]. The β-strand type hydrogen-bonding pattern, while uniquely defined, has non-ideal geometry and hydrogen bonding between monomers to form the channel structure needs to be explicitly incorporated. Furthermore, in sidechain packing there are significant van der Waals contacts between some of the sidechains as each sidechain structure has been determined independently. In addition, the sidechain structures have been built upon the initial backbone structure and any modification to the backbone will necessitate changes to the sidechains. Moreover, the covalent geometry was fixed for this initial structural characterization. The peptide linkages have been restricted to planar structures even though preliminary data analysis suggests that a significant deviation from planarity may

Figure 1

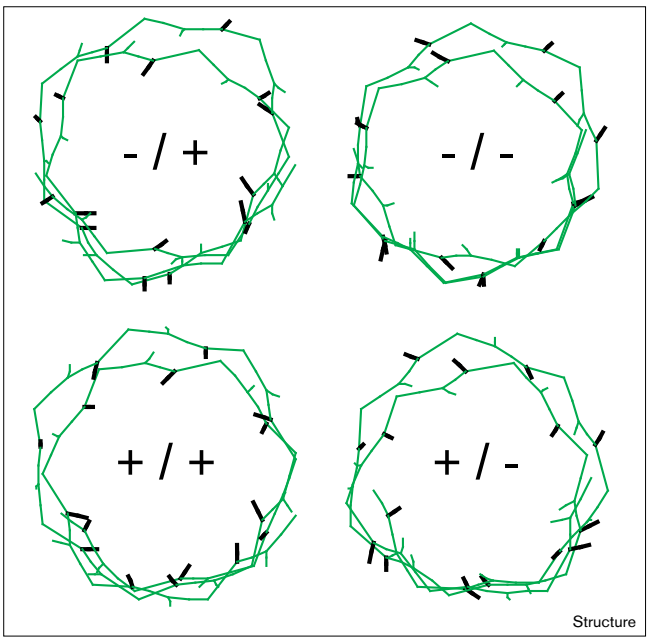

A set of four initial structures defined solely from the NMR data and an assumed covalent geometry [36]. These structures represent the full range of chirality ambiguities [37]. (+/–) represents a pattern of alternating peptide plane orientations having the formyl and even-numbered amino acid C–O bond directions oriented slightly in towards the helical axis (+) and the odd-numbered amino acid C–O bond directions oriented slightly away from the helical axis (–). The other three structures represent permutations on this theme. All of these structures have the same hydrogen-bonding pattern, helical sense and number of residues per turn.

exist for many of the peptide linkages [45]. For these reasons and with the goal of solving the chirality ambiguities the structure has been refined using a protocol described here that evolved from preliminary computational efforts [16,17]. Not only will refinement yield a solution to the above problems, but in this process all of the orientational constraints can be equally weighted. No definitive effort has been made in this refinement, however, to uniquely characterize the few sidechain 'most probable' torsion angles, although extensive conformational space has been searched, as will be demonstrated.

The strategy for refining the structure involves setting up a generalized global penalty function that incorporates all available experimental data (weighted equally based on experimental error) for the backbone and sidechains, the intramolecular hydrogen-bond distances and the full CHARMM empirical energy function [1]. The refined structure is obtained from a geometrical search using the search algorithm to obtain the minimum described by this global penalty function. Because the structural constraints are very precise, the penalty between possible conformational states is high making the search between local conformational states difficult. Therefore, simulated annealing is used to perform the minimization of this penalty function in such a high-dimensional configuration space [46,47]. Modifications to the structure are made by allowing the complete geometry of the polypeptide to vary through modifications of the atomic coordinates and changes in peptide plane orientations [17]. These orientations were changed through compensating moves involving small equal but opposite sign changes to ψ_i and ϕ_{i+1} and through tunneling moves in

Figure 2

Distance difference matrix plots [43,44] illustrating the structural differences between the four initial structures. Distances between all backbone atoms in the polypeptide are placed within a matrix for each structure. The matrices are subtracted to achieve the difference maps in which cyan represents a positive difference and magenta a negative distance difference.

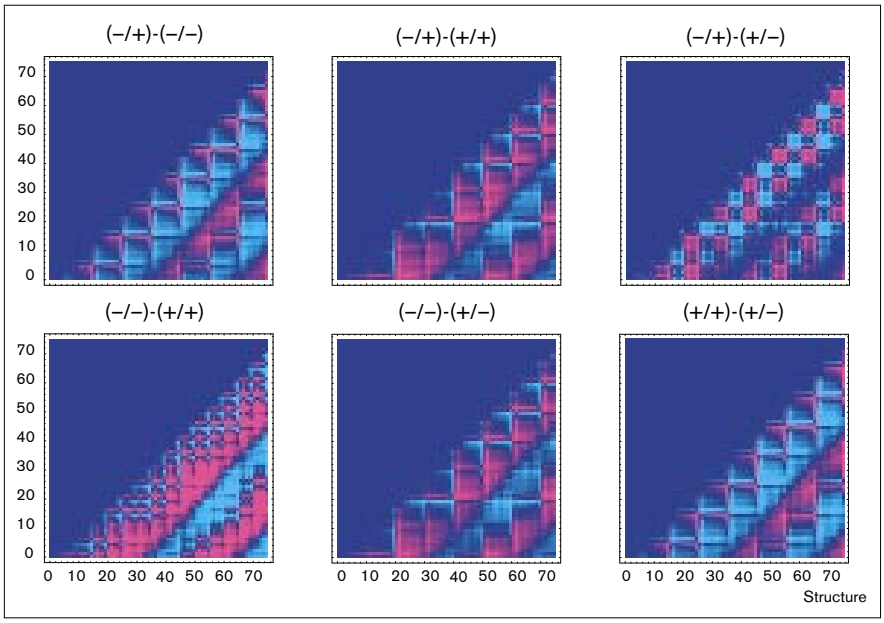

which the direction cosine of the peptide plane normal changes sign as modeled by a potentially large ψ_i and ϕ_{i+1} compensating move. The resulting high-resolution structure demonstrates a novel approach for achieving a high-resolution structure as well as providing numerous insights into the details of cation solvation and channel conductance.

Results

Refinement of initial structures

The refinement of each of the four initial structures was repeated ten times starting with a different random number seed to ensure ten different refinements. The different refinement ensembles of superimposed structures are shown in Figure 3. Each ensemble shows a very high level of self consistency with regard to the atomic positions (all atom root mean square deviations (rmsd) of 0.15, 0.15, 0.11 and 0.17 Å for (–/+), (–/–), (+/+) and (+/–), respectively). Also shown in Figure 3 are the backbone C–O orientations. For each residue the starting orientation reflects the chirality ambiguities and is shown as a horizontal line. The circles in each track represent the C–O bond orientation for each of the ten refinements. With few exceptions, the orientation of individual carbonyls is defined within a precision of approximately +/– 3° in the individual ensembles. The exceptions have two discretely populated states, for instance, Trp11 in the (+/+) ensemble has the C–O orientation populated around +10° and around –20°. Furthermore, there is a high degree of correlation between ensembles indicating that the refined structure is independent of the chirality choice in the initial structure. This suggests that conformational space for the two chirality possibilities is being adequately searched in the refinement procedure. In Figure 4 an example of a C–O bond orientation trajectory during refinement is shown. The affect of the tunneling moves is clearly demonstrated as jumps across the C–O orientation of 0°. In addition, relatively large changes in C–O orientation resulting from compensating torsional moves are illustrated as changes in C–O orientations over a large number of steps. By way of example, for a single refinement 562,588 moves were attempted in the ratio of 30:50:20 for atom, compensating and tunneling moves, respectively. Of these only 90,456 moves were accepted in the ratio of 52:47:1, respectively, reflecting the amplitude of the moves.

The refinement trajectories (not shown) for the dipolar constraints start at zero penalty, because the initial peptide plane orientations are defined by the dipolar data, while the chemical shift refinement trajectories do not start with perfect agreement between the observed and calculated values. While excursions outside of the experimental error range are made for all data types, the difference between experimental and calculated values of the observables is eventually minimized. This emphasizes that the refinement is against all of the data and that the structure is not biased towards one or two of the observables. The penalty for these selected data types and for the energy is minimized and comes to an equilibrium, but non-zero level. The non-zero values of the experimental data are, however, within experimental error limits and therefore, the experimental data is parameterized properly in the penalty function.

The penalty distribution is shown in Table 1 for both the initial and refined structures. The penalty values have been multiplied by the λ values indicated for each penalty type and reflect the penalty used during the refinement. The initial structure penalty is dominated by the quadrupolar splittings and the CHARMM energy, and more specifically the van der Waals contacts. The penalty from quadrupolar splittings is dominated by the leucine sidechains that have been energy minimized from their analytical solution to avoid excessive overlap with the tryptophan sidechains. During the refinement the penalties associated with the experimental data are reduced except for the penalties associated with the dipolar interactions which were used to define the initial structure. The breakdown of the energy penalty (Table 1) is spread over many contributing factors with the angle energy, electrostatics and dihedral components contributing the most. The van der Waals interactions which dominated the initial structure have been reduced to very small components of the final penalty. Even the significant contributors to the energy penalty do not represent major contributions from single atomic sites, but rather numerous small influences and consequently there is no indication that the structure is in a local or false minimum.

The structural ensembles can also be compared with each other. A matrix for each ensemble is constructed using rms distances in the upper left half of the matrix and average distances in the lower right half. The difference matrices (Figure 5) show that the significant differences between initial structures have almost completely disappeared with the exception of the (+/–) ensemble. Even in this ensemble the distance differences are associated with a single peptide plane (containing the carbonyl of Trp13) that has a different chirality than the other three ensembles. The atomic rmsd between all 40 refined structures is 0.48 Å even though these refinements started from four different starting structures.

Final structure

To achieve a single refined structure, an average atomic structure of the four ensembles (shown in Figure 3) was formed by first superimposing all 40 structures. All of these structures were used for the average because the total penalties for each refinement vary over a relatively narrow range from 411 to 513 with no significant outliers. Taking an atomic average distorts the bond lengths and bond angles as well as the structural orientation used in calculating the orientational constraint values, so refinement of the average structure is required. As only minor distortions in

Figure 3

Initial structure refinements. The four initial structures were each refined ten times to produce 40 refined structures. The four ensembles were generated by superimposing the structures through rotation about Z and translation in X and Y. Rotation about X and Y would change the penalty value associated with the orientational constraints and was therefore not allowed. The structures within each group show little variability in the atomic positions. The carbonyl orientations with respect to the channel axis were monitored for each refinement group to determine the ability of the refinement procedure to reach a global refined structure. Positive angles were defined for the C–O bond oriented in towards the helical axis; (o) represents the C–O orientation in each refined structure and (–) represents the C–O orientation in the initial structure.

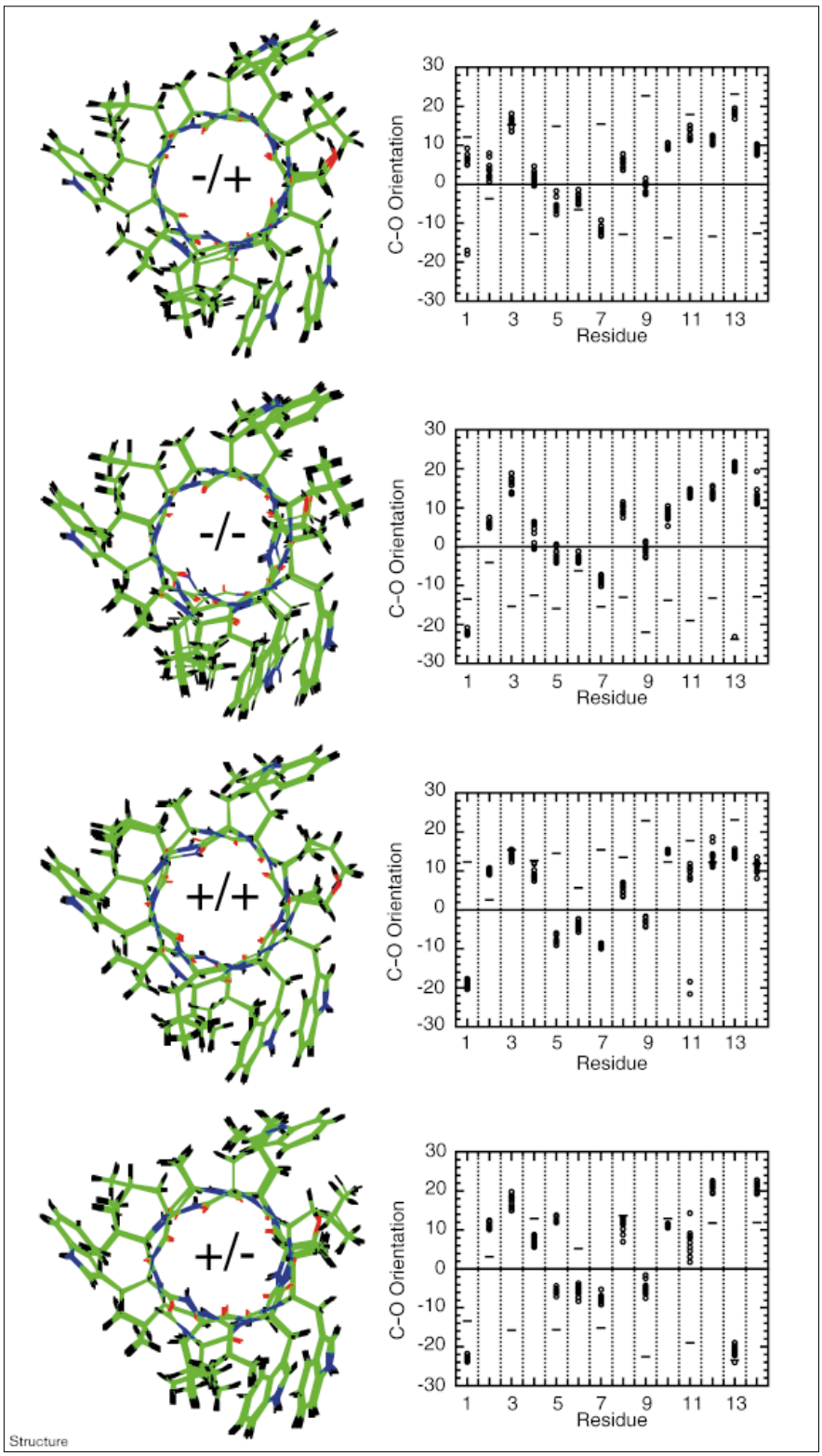

the structure are generated, atom moves alone were used in this final step of the refinement with a modest starting temperature and a 5×10^{-4} Å diffusion parameter. The final structure has a penalty of 389 (Table 1) and only minor

Figure 4

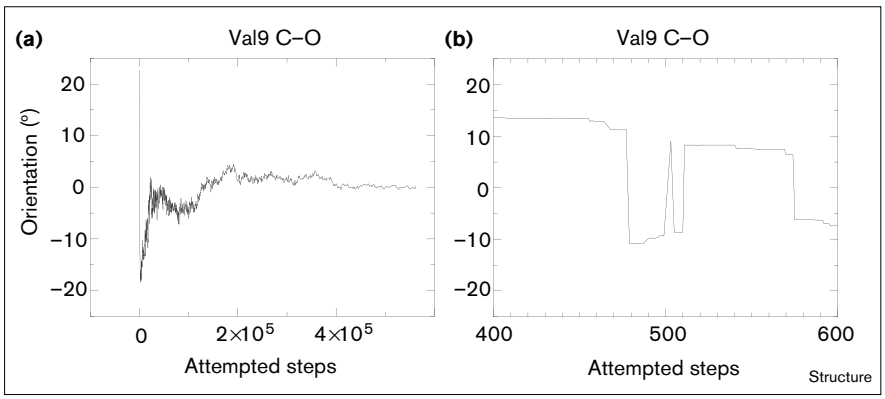

Typical backbone C–O orientation trajectory. **(a)** The full refinement and **(b)** an expansion of an initial portion of the trajectory. This initial structure (–/+) had a C–O orientation of +22° and after a combination of tunneling, compensating and atom moves the refined orientation for the Val9 C–O orientation is 0°.

structural changes have occurred upon refinement, as documented by an atomic rmsd between the averaged and final structure of 0.32 Å. Repeating this refinement protocol generates a nearly identical result, but repeating the protocol without the experimental constraints as contributors to the penalty, results in substantial deviation from the experimental observables as shown in Table 1. While the energy penalty is somewhat lower the penalty associated with the experimental data is much greater.

The final structure is shown in Figure 6. This structure represents all of the experimentally derived structural constraints used in the refinement procedure, the intra- and intermolecular hydrogen bonds as well as CHARMM energy. While the initial structures had a fixed covalent geometry, the final structure shows subtle differences in this geometry. For example, the N–C_1 bond lengths, initially set at 1.34 Å, refine to a range from 1.325 to 1.364 Å with the average remaining at 1.34 Å. The N–C_α–C_1 bond

Table 1

Penalty distribution for the initial, initial refined, averaged and final refined structures.

	Initial refinement All constraints			Final refinement All constraints			Final refinement Just energy	
Penalty type*	λ	Initial penalty	Refined penalty	λ	Average structure penalty	Final structure penalty	λ	Final structure penalty†
^{15}N CS	3.0	23.1	1.2	3.0	16.9	0.9	0.0	11.7
^{13}C CS	3.0	0.4	0.1	3.0	0.1	0.0	0.0	0.2
^{15}N Indole CS	3.0	7.2	0.2	3.0	0.1	0.1	0.0	17.8
^{15}N–$^{13}C_1$ DS	3.0	0.2	1.7	3.0	10.3	1.4	0.0	58.0
^{15}N–^{1}H DS	3.0	0.4	1.7	3.0	5.7	2.2	0.0	6.7
^{15}N–^{1}H Indole DS	3.0	4.4	0.6	3.0	0.4	0.5	0.0	0.2
^{2}H QS	3.0	4961.7	8.9	3.0	313.6	6.0	0.0	1384.7
Distance	3.0	85.1	9.8	3.0	13.0	7.7	0.0	11.6
CHARMM Energy	1.0	3400.9	396.7	1.0	5623.2	370.2	1.0	243.1
bonds	1.0	45.1	18.1					
vdW	1.0	2331.9	5.5					
vdW (image)	1.0	601.8	−7.5					
electrostatics	1.0	102.9	92.3					
electrostatics (image)	1.0	73.1	67.9					
angles	1.0	109.8	122.1					
Urey-Bradley	1.0	8.9	15.0					
dihedrals	1.0	72.4	78.6					
impropers	1.0	0.1	4.0					
CM‡	1.0	55.0	0.9					
TOTAL Penalty		8483.4	420.9		5983.3	389.0		1734.0

*CS = chemical shift; DS = dipolar splitting; QS = quadrupolar splitting. †Obtained prior to multiplying by λ. ‡Center of mass (CM) for constraining the structure along the Z axis.

Figure 5

Distance difference matrices (as described in Figure 2) between the refined ensembles of the four initial structures. Each ensemble is characterized by root mean square (rms) and average distances between each of the backbone atomic sites. Rms differences are shown in the upper left half of the plots and average distance differences in the lower right half of the plots.

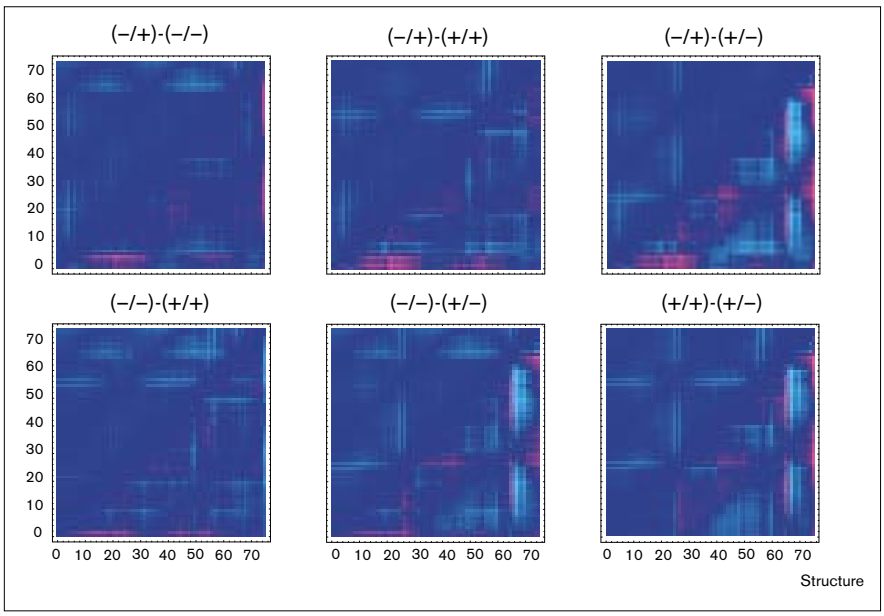

angle, originally set to 110°, refines to a range of 105.5 to 113.9° with an average of 109.4°. However, there are a few angles, typically about the C_α carbon, that have been modified by the refinement protocol to a value greater than 2.0 standard deviations from the mean, as defined by PROCHECK [48] and Engh and Huber geometry [49]. These outlying bond angles appear to be randomly dispersed in the structure and do not represent a systematic problem with the refinement protocol.

The ϕ, ψ torsion angles in the backbone have changed by as much as 30 to 35° upon refinement (Table 2), but most of these changes are compensated for by peptide plane changes to ψ_i and ϕ_{i+1}. The ω torsion angles, which were fixed at 180° in the initial structures, clearly show considerable nonplanarity in the refined structure. Three peptide planes are twisted by more than 10°, one by 15.4° and all by an average of 6.2°. These results show that the assumption of peptide linkage planarity introduces a significant error for the analysis of such structural constraints. During the refinement the carbonyl orientation and hence the chirality ambiguities are uniquely defined. The result is that most of the carbonyl orientations are positive (Figure 7), that is with the carbonyl oxygen oriented in toward the channel pore. The unique solution for these carbonyl orientations has been made possible by the tunneling moves in the refinement protocol. It is, however, uncertain which constraint (energy or experimental data) forced the unique solution for these carbonyl orientations.

The helical pitch and residues per turn have been calculated from an analysis of the C_α carbon coordinates (Figure 8). The X and Y coordinates orthogonal to the bilayer normal and the channel axis display a sinusoidal periodicity that has been simulated using the equation:

$$n = a + b \sin (cx + d)$$

where 'n' is the X or Y coordinate, 'a' is a minor correction for the location of the channel axis and b ≅ 4 Å is the radius of the channel as measured to the center of the C_α carbons. The van der Waals radius of the pore is closer to 2 Å and is constrained primarily by the amide atoms. The parameter 'd' controls the phase of the sine wave and differs slightly from 90° for the X and Y plots (actually 91.6° for these independent simulations). The parameter 'c' defines the number of degrees per residue, which is 55.5 and 55.3°, from the X and Y plots, respectively; this translates to 6.48 and 6.51 residues per turn. Early models of the gramicidin A channel [50] described the helix as a $\beta^{6.3}$ helix for 6.3 residues per turn. This represents a small but significant difference in the experimental structure, but does not represent a different hydrogen-bonding pattern. The Z axis coordinates show minor fluctuations reflecting the dipeptide repeat unit, but the data is fit to a straight line with a slope of 0.76 Å per residue which is equivalent to 4.9 Å per turn, the helical pitch of the gramicidin A channel. The H–O and N–O hydrogen-bond distances have been brought within the assumed error range of ± 0.3 Å. Furthermore, the N–H distance (assumed to be 1.0 Å) plus the H–O distance is approximately equal to the N–O distance, suggesting that the N–H–O angles are small.

Figure 6

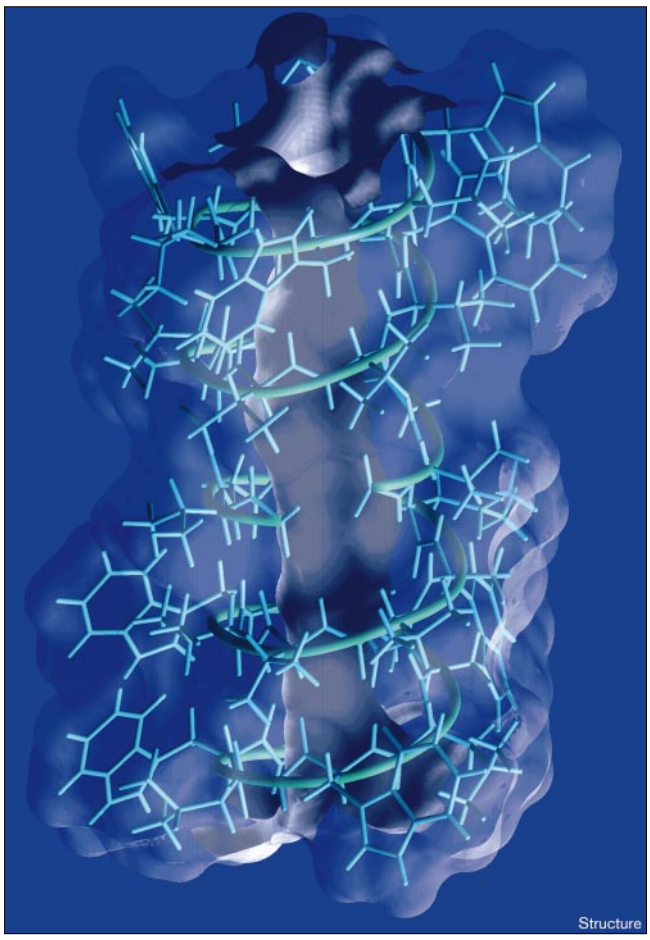

Final structure of the gramicidin A channel structure based on the refinement described in this paper. The external and internal Connolly surfaces were rendered using a probe sphere of radius 1.4 Å. The light source is positioned at the bottom of the figure to shine through the pore. The all-atom stick representation was prepared using Insight II and the structure is oriented so that the formylated N terminus to N terminus junction is visible in the center of the figure.

The changes in sidechain torsion angles are also small with only a single change in rotameric state. The Leu10 initial structure has $\chi_2 = -12°$, an essentially eclipsed conformer, but prior to refinement the sidechains of Leu10, Leu12, and Leu14 were energy minimized. While this procedure only modified the torsion angles of Leu12 and Leu14 slightly, the Leu10 χ_2 angle in the four initial structures ranged from –75° to +86°. Refinement led to a unique rotameric state with a χ_2 angle of –71°. Consequently, a significant search of sidechain conformational space has occurred. While the search was substantial, the changes in torsion angles for other residues were small. The only other sidechain torsion angle to change by more than 10° was Trp9 χ_2 (changed by 15°) and this residue was directly affected by the significant change in Leu10.

While inclusion of the CHARMM structural energy has been essential, it influences the structure in a way that may not correspond exactly to the influence from the experimental data. The energy is calculated for the molecule in a vacuum while the experimental data has been obtained from a hydrated lipid bilayer environment. The penalty due to the experimental data is reduced to a point that is very close to zero, and cannot be further reduced. While the calculated energy is significantly reduced during refinement, it can be reduced further in the absence of the experimental constraints (Table 1). This indicates that although the penalties from the two different types of constraints are both necessary and are reduced during refinement, they compete for control of the structural modifications.

Discussion

Orientational constraints

Orientational constraints derived from solid-state NMR of uniformly aligned samples have been used to define initial structures and as precise structural constraints throughout the refinement. Such constraints are not only adequate for defining a three-dimensional structure, but the structural model is constrained to very high resolution, especially compared to other membrane protein structures (e.g., [51–54]). The solution NMR derived nuclear Overhauser effect (NOE) constraints represent second order relaxation quantities. Changes in spin populations result in a perturbation of coupled-spin populations that yield the NOE. Unlike this second order effect, the orientational constraints correspond to first order average Hamiltonian quantities and consequently, based on first principle arguments, the orientational constraints will generate more accurate structural constraints and hence higher resolution structures.

The accuracy of these constraints is confirmed by the lack of distorted covalent geometry in the final structure. For two of the peptide linkages the structure is constrained by ^{15}N and $^{13}C_1$ chemical shifts, ^{15}N–^{1}H and ^{15}N–$^{13}C_1$ dipolar interactions as well as C_α–^{2}H quadrupolar splittings. Such an array of data over determines the orientation of this pseudo-plane. If the nuclear spin interaction tensor element magnitudes and orientations were not accurately known then the data would distort the covalent structure during refinement and this is not observed. Therefore, the constraints are both precise and reasonably accurate. Moreover, the assumptions that have been made about these tensors are shown by this result to be reasonable [55].

The most unique feature of these constraints is that the errors associated with each constraint do not sum as the structure is assembled [36,56]. This is because each constraint orients the molecule with respect to the laboratory frame of reference, an absolute constraint, whereas distances between atomic sites within a macromolecule, such as NOE constraints, represent relative constraints. Therefore, each orientational constraint is an independent structural

Table 2

Initial and final structure torsion angles.

Residue	ϕ	ψ	ω	χ_1	χ_2	χ_3
Initial (+/−) structure						
Val1	−139	141	180	−178	–	–
Gly2	127	−117	180	–	–	–
Ala3	−130	153	180	–	–	–
Leu4	120	−103	180	−154	160	–
Ala5	−142	151	180	–	–	–
Val6	123	−116	180	55	–	–
Val7	−132	150	180	−145	–	–
Val8	119	−104	180	55	–	–
Trp9	−135	152	180	−72	−97	180
Leu10	108	−98	180	−58	−12	–
Trp11	−134	146	180	−70	−81	180
Leu12	114	−101	180	−173	−61	–
Trp13	−134	153	180	−63	−90	180
Leu14	110	−101	180	−173	−63	–
Trp15	−136	155	180	−58	−96	180
Final structure						
Val1	−108	121	171	177	–	–
Gly2	151	−129	176	–	–	–
Ala3	−115	144	−174	–	–	–
Leu4	122	−136	−173	−157	152	–
Ala5	−116	125	−179	–	–	–
Val6	147	−118	176	59	–	–
Val7	−120	126	165	−151	–	–
Val8	152	−120	178	60	–	–
Trp9	−111	128	−173	−74	−82	171
Leu10	129	−128	176	−73	−71	–
Trp11	−109	152	168	−71	−91	−174
Leu12	114	−119	175	−177	−59	–
Trp13	−100	153	167	−64	−85	176
Leu14	111	−115	178	−176	−72	–
Trp15	−108	127	−178	−61	−90	176

The torsion angles for the initial (+/−) structure are before energy minimization.

constraint, while distance constraints are dependent structural constraints. Consequently, when the polypeptide backbone structure of gramicidin A was assembled, the hydrogen-bonding geometry between residues i and i+6 was reasonable despite a couple of degrees error in each of the fourteen dipolar constraints between the i and i+6 residues. Therefore, despite the very local nature of these constraints, reasonable secondary structure and short range tertiary structure could be described from orientational constraints.

Refinement

The refinement procedure described here introduces only minor structural perturbations leading to a structure that encompasses the experimental data, minimizes the calculated structural energy and optimizes the hydrogen-bond geometry. The simultaneous use of experimental data and energy as contributors to the penalty function produces a refined structure that satisfies well all imposed constraints without being overly biased toward either the data or the energy. This also means that all constraints are satisfied by minor changes in the initial structure. This is not to say,

Figure 7

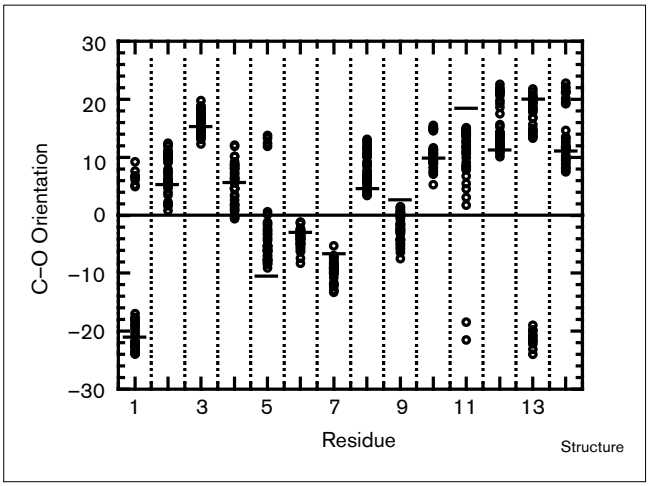

Carbonyl orientations (as described in Figure 3) for the superposition of the 40 refined structures (o) and for the final refined structure (–).

Figure 8

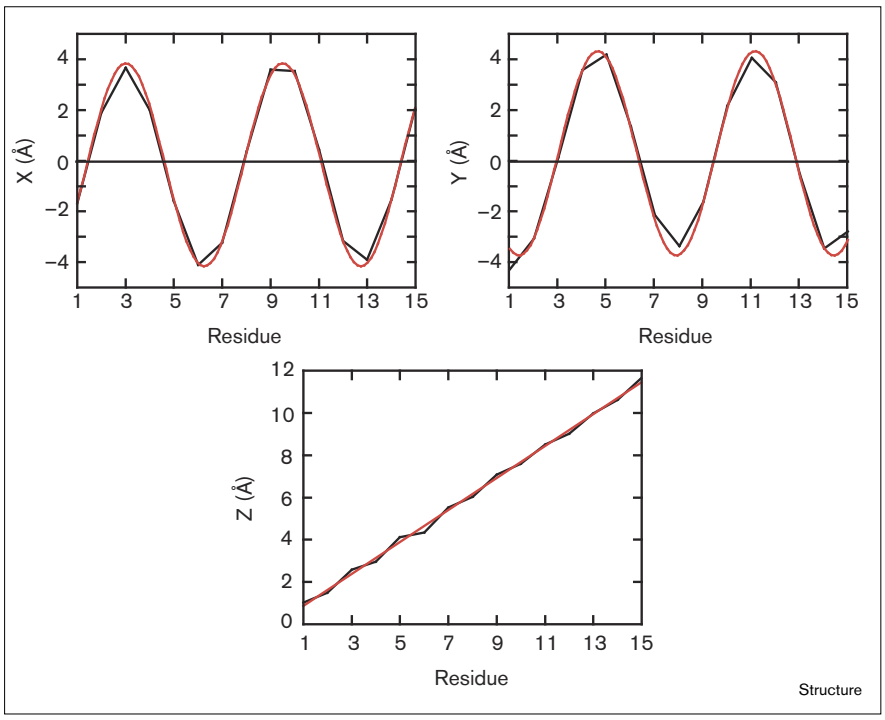

Helical parameters defined by C_α location. The C_α coordinates in X, Y and Z plotted against the C_α residue numbers yields information concerning the helical parameters, such as the number of residues per turn and helical pitch (see text for details).

however, that the changes are insignificant. In refining the structure, the covalent geometry has been relaxed, the van der Waals contacts have been relieved and the peptide linkages have been allowed to become nonplanar. Most importantly, the chirality ambiguities in the backbone have been resolved. The final orientations of the carbonyl groups, either into or away from the pore, have been shown to be independent of the starting orientation. This finding suggests that the performed conformational search in torsion angle space using this set of constraints is adequate to define a unique structure. The result of the initial 40 refinements (Figure 7) shows that the carbonyl orientations are typically defined to within ± 5°. This describes a high-resolution structure that permits the drawing of biological implications. At the same time this structure is a time averaged or motionally averaged structure. The precision with which the torsion angles are defined does not imply that dynamic amplitudes are less than, or equal to, the error of the structural determination. In fact, librational amplitudes of the peptide planes have been shown to be as great as ± 20° [57]. This is a high-resolution characterization of a motionally averaged structure.

High resolution channel structure

There have been numerous gramicidin A structures published. These structures fall into two categories: the double helical structures that occur in organic solvents and rarely in lipid bilayers [58,59]; and the single-stranded dimeric state that has only been observed in lipid and detergent environments. The only experimentally derived structure of the single-stranded dimer, other than that presented here and in our earlier preliminary results, was derived by solution NMR in sodium dodecyl sulfate (SDS) micelles [7,8]. These two structures have the same hydrogen-bonding pattern and hence polypeptide fold, but details of the backbone structure cannot be easily compared because the solution NMR structure is not a high-resolution structure and because this structure was refined with the ω torsion angles fixed at 180°. Nevertheless, there appears to be significant differences in the sidechain rotameric states for Trp9, Leu10, Leu12 and Leu14. Furthermore, the dynamics of the polypeptide appear to be different in these two environments. In micelles, multiple χ_1 rotamers for Val7 are populated and χ_2 rotamers for Leu4 and Leu12. In bilayers, multiple χ_1 rotamers for Val1 and Val7 are populated and both χ_1 and χ_2 for all of the leucine residues are fixed in single rotameric states. These differences are not surprising as the hydrophobic/hydrophilic surface of the two environments is so different: a curved micellar surface for the solution NMR studies and a planar bilayer surface for the solid-state study.

As mentioned above, the high-resolution structure affords an opportunity to study many of the functional details of this ion channel. The four tryptophan residues have several functional roles. The indole N–H groups are all oriented toward the bilayer surface and all can undergo $^1H/^2H$ exchange with the aqueous solvent [41]. Presumably, these

sites are hydrogen-bonded at the hydrophilic surface, thereby helping to orient the channel with respect to its anisotropic membrane environment. Hydrogen bonding of the indole NH groups to the phospholipid carbonyl and to water molecules in the bilayer interface has been observed in molecular dynamics simulations of the gramicidin A channel incorporated in a dimyristoylphosphatidylcholine (DMPC) bilayer [25]. When phenyl groups replace the indoles, the gramicidin monomers (gM) are known to 'flip-flop' between the bilayer leaflets, a dynamic process that does not readily occur when the indoles are present (OS Andersen and coworkers, personal communication). Consequently, the indoles function to both orient the channel to the bilayer surface, so that the molecule can conduct cations, and to stabilize this structural orientation.

The indoles are also essential for forming the single-stranded dimer that is the conducting state [59]. The most common state in nonpolar organic solvents is an antiparallel, intertwined, double helical dimer that has been well characterized by crystallography and solution NMR in organic solvents [2,3,6]. Such a structure has a relatively even distribution of indoles over its surface and, while stable in low dielectric isotropic solvents, it is not stable in the heterogeneous lipid environment where the indoles prefer the bilayer interface rather than the low dielectric interstices of the bilayer. When tryptophan is replaced by phenylalanine, the channel state becomes a relatively rare event in lipid bilayers, instead an antiparallel double helical structure dominates [59,60], the same structure that is present in low dielectric isotropic solvents. Consequently, the indoles destabilize double helical conformers in a lipid environment, while stabilizing the conducting state. It also appears as if the indoles are one of the factors involved in determining the handedness of the channel-state structure (W Hu, M Cotten and TAC, unpublished results). The indoles have a preferred orientation at the bilayer hydrophobic/hydrophilic interface with the N–H oriented towards the bilayer surface and the benzyl ring oriented into the hydrophobic domain. Such an optimal orientation is only possible for each of the indoles if the structure is right-handed. Other factors also appear to be important in determining the channels handedness, because when gM does form the channel structure it predominantly forms the right-handed structure [61].

Experimental evidence has been presented suggesting that the dipole moments of the indoles have a direct effect on ion conductance [29,41]. From a knowledge of how the indoles are oriented and their distance from the center of the channel at the bilayer center, it is possible to calculate the electrostatic influence of these dipoles on a cation (monopole) at the bilayer center. Despite distances of 10–12 Å, the low dielectric environment of the bilayer interstices allows for a significant electrostatic effect that accounts for a reduction in conductance by a factor of 20 when phenyl groups replace indoles. The radial components of the dipole moments help stabilize cations in the channel and the tangential components may also be important for cation translocation. While molecular modeling has suggested that the path of the cation through the gramicidin A channel may be helical [62], experimental evidence has only recently supported this concept [63]. A helical path means that the cation moves through the channel off axis, that is the cation does not pass down the center of the channel, but rather follows a path likened to a spiral staircase. As a result the tangential components of the indole and backbone dipoles may be important for facilitating cation translocation.

The location of the carbonyl groups along the helix axis is crucial for modeling cation conductance. During the refinement, the alternating or uniform pattern of carbonyl orientations (into or out of the pore) in the initial structures was disrupted, bringing many, but not all, of the carbonyl oxygens in towards the channel axis. The gramicidin A channel pore supports a single-file column of water molecules and during cation conductance one of the water molecules is replaced by a cation. Consequently, much of the primary hydration sphere is stripped from the cation as it enters the channel and presumably the carbonyl oxygens provide the necessary solvation environment for the cations [62,64–68]. Therefore, the inward orientation of ten of the 14 carbonyl oxygens (Figure 7) is functionally important. Furthermore, the carbonyls at the C termini, which form a cation-binding site, show the greatest tilt in towards the channel axis, as had been predicted [68,69]. Carbonyls of Leu10, Leu12 and Leu14 provide oxygens that are primarily involved in the cation-binding site [63,70]. The position of these carbonyls is consistent with both the scattering studies, showing that the binding site is 9.6 Å from the bilayer center [71], and with an analysis of $^{13}C_1$ orientational constraints and molecular dynamics that place the binding site at 9.2 Å from the bilayer center [72]. The carbonyl orientations are consistent with our understanding of cation binding and with the potential energy surface for cation conductance which has two minima and three maxima, the central maximum representing the rate-limiting step [41]. It is, however, surprising that the refinement has shown such a preference for unique chirality solutions when the energy has been calculated without water molecules in the channel. This suggests that whatever constraint is dictating carbonyl orientations the constraint is robust and if it is the CHARMM force field it is not dependent on interactions between the polypeptide and solvent in the channel. Whatever the cause, it does not appear to be an artifact of the refinement protocol, as the amide exchange data from the polypeptide backbone of the channel-state in lipid bilayers also supports this pattern of carbonyl orientations [73]. The exchange data is sensitive to the extent of N–H exposure to the solvent, such that the N–H groups oriented towards the bilayer surface or channel pore, exchange more readily.

Evidence has also been presented recently showing that the carbonyl orientations do not change significantly upon cation binding [74,63]. Because the positions of the carbonyls are precisely known, modeling of Na^+ ion in the channel further suggests that two carbonyls, rather than three or four, are involved in solvating the cation at any one time and that the Na^+ ion is positioned off the center axis of the channel in order to form optimal electrostatic interactions with the carbonyl oxygens.

The high-resolution structure provides a precise framework on which to build an experimentally defined description of molecular dynamics. The backbone dynamics have been extensively characterized by temperature-dependent powder pattern analysis [57] and by field-dependent T_1 relaxation times [75]. Motions occurring on the ten nanosecond timescale were characterized. This is the same timescale as cation translocation from one carbonyl site to another along the pore, as estimated from conductance measurements [76], suggesting that a correlation between molecular dynamics and the kinetics of cation passage may occur in the gramicidin A channel. In fact, all of the water molecules must move coherently with cations during cation translocation, because of the single-file nature of the water molecules in the pore. What these dynamic characterizations suggest is that the coherence is not restricted to molecules in the channel, but also includes the backbone of the channel.

Biological implications

Membrane-bound or membrane-associated proteins represent approximately 30% of all human genome products. Few structures of such proteins have been determined, and none at high resolution. A new approach in using solid-state nuclear magnetic resonance (NMR) of uniformly aligned bilayer preparations is demonstrated here for the determination of a high resolution polypeptide structure in a lamellar phase lipid environment. For this procedure, neither crystallization for X-ray diffraction nor isotropic solutions for solution NMR studies were required. Instead bilayer films between glass plates yield very well oriented samples. As membrane proteins contain a high percentage of α helix approximately parallel to the bilayer normal it should be possible to achieve uniform magnetically aligned samples of these proteins.

The high-resolution structure of the gramicidin A channel has led to the characterization of specific peptide–bilayer interactions, peptide–cation interactions and a fundamental understanding of cation solvation by a channel pore. Such understanding was not achieved previously, even though models of the polypeptide were well established. In particular, the recognition that little structural deformation takes place when the largely desolvated cation interacts with the channel is a novel and essential concept for efficient channel conductance [63]. If an ideal cation-binding site existed in the channel considerable energy would be needed to move the cation through the channel. Instead adequate, but not ideal cation solvation is utilized in gramicidin A. Moreover, it is likely that this principle applies to the proteinaceous cation channels that currently represent a major structural frontier. The use of a high-resolution structure demonstrated here makes this frontier even more challenging, as many of the functional secrets of membrane channels will be solved only through high resolution structural and dynamic characterizations.

Materials and methods

The application of simulated annealing to this global optimization problem requires a definition for the system configuration, a method by which the configuration is varied and a penalty function by which the structural variations are controlled. The four structures shown in Figure 1 were used as the basis for the initial system configuration, but as there are significant van der Waals contacts involving the sidechains of Leu10, Leu12, and Leu14, these leucine sidechains were energy minimized while the backbone and all other sidechains were fixed in position. This was accomplished using 250 steps of adopted basis Newton–Raphson minimization [77] with CHARMM.

To search the necessary conformational and local structural space, both atom and torsional modifications were implemented. Random atom moves with a small diffusion parameter of 5×10^{-4} Å in each of three cartesian axes relaxed to the atomic geometry and helped minimize the global penalty. Torsional moves were generated in two forms, compensating moves and tunneling moves. Compensating moves involve simultaneous changes to ψ_i and ϕ_{i+1} of equal magnitude and opposite sign [78]. They were used so that the helical parameters would remain essentially the same while the torsion angles were modified by a random amount up to $\pm 3°$ per step. This was necessitated because noncompensated torsional moves result in tipping part of the helix and generating large penalties from the experimental constraints. These compensating moves essentially rotate the peptide planes about the C_α–C_α axis. Tunneling moves are a specialized version of the compensating moves designed to search conformational space about the two chirality solutions [37]. The magnitude of the tunneling adjustments are calculated so that the magnitude of cos θ, the angle of the peptide plane normal with respect to B_o, remains the same, but the sign of cos θ is changed. These moves were needed in order to transit the penalty barrier at $\cos\theta = 90°$, which is often substantial. The ratio of attempted compensating, tunneling and atom moves used in the refinement reported here was 0.5:0.2:0.3. This ratio and other annealing parameters were optimized through consideration of the final experimental and energy penalties.

The penalty function used to control the structural refinement is the sum of the structural penalties plus the energy, where each structural penalty refers to a particular data type (e.g. ^{15}N chemical shift) and

$$\text{Total penalty} = \sum_{i=1}^{M} (\lambda_i \cdot \text{Structural penalty}_i) + \lambda_E \cdot \text{Energy} \qquad (1)$$

where M is the number of structural penalties and λ is a scaling factor. λ_i was set to 3.0 and λ_E to 1.0 for the refinement protocol used here. The individual structural penalties are calculated as:

$$\text{Structural penalty} = \sum_{j=1}^{N} \frac{1}{2} \left(\frac{\text{Calculated}_j - {}_j\text{Observed}_j}{\text{Experimental error}_j} \right)^2 \qquad (2)$$

where N is the number of measurements of a specific data type.

The use of the experimental error in the definition of the total penalty serves several purposes. In so doing the various data types are normalized by the frequency units and the magnitude of the error bar. In other words, the magnitude of each experimental error is relative to the observed interaction size and, therefore, division by the error has the result of both scaling the different data types so that they contribute equally to the total penalty and making the penalty for the individual data types dimensionless. In this way each structural constraint is weighted appropriately and one of the more significant problems associated with the initial structure is overcome. It is also important to have the ability to define separate error values within a particular data type, as experimental error may vary from site to site depending on the quality of the data.

The penalty function describes a parabolic well, such that a structural deviation resulting in a difference between the experimental and calculated observables is quadratically penalized based on the magnitude of the difference. It has been suggested [79] that this type of function will lead to conformational pinning, which is true for data that is not well defined such as NOEs. For this solid-state NMR (SSNMR) data however, the observed values are quite accurate with small experimental errors. As a result, the SSNMR data can all be accommodated without significant conformational pinning. A flat bottom function was initially used and it was seen that the structural fit to the experimental data was not as good.

The constraints imposed on the structure during refinement are 19 ^{15}N and two $^{13}C_1$ anisotropic chemical shifts, 14 ^{15}N–$^{13}C_1$ and 19 ^{15}N–^{1}H dipolar splittings, 12 C_α–^{2}H and 54 other quadrupolar splittings, ten N–O and ten H–O hydrogen-bond distances and the energy for a total of 141 constraints. The observed chemical shifts are compared to calculated chemical shifts obtained from the molecular coordinates and the known tensor orientation and tensor element magnitudes [17,55,57,80]. A change in the orientation of the atomic coordinates leads to a change in the calculated chemical shifts and a resultant change in the penalty. Similarly, observed dipolar and quadrupolar splittings are compared to calculated values derived from the atomic coordinates and a knowledge of these interaction tensors in the molecular frame of reference.

The initial structure readily identifies the intramolecular hydrogen bonds (on average these are within 0.5 Å of ideal β sheet hydrogen-bond distances). The hydrogen bonds are therefore included as direct contributions to the penalty function, as is routinely the case in structural refinements from solution NMR [81,82]. During the refinement, the intramolecular hydrogen-bond distances are calculated and compared to generally accepted H–O and N–O distances for β-sheet structures (1.96 ± 0.3 Å and 2.91 ± 0.3 Å, respectively [83]). The large range of acceptable distance values serves to constrain the hydrogen bonding without presuming the final structure.

The all-atoms PARAM22 [1] version of the CHARMM force field was used to describe the internal energy (bond lengths and angles, and dihedral angles), as well as the nonbonded interactions (van der Waals and electrostatics). While translation in X and Y have no bearing on the calculations of the SSNMR observables, such translations interfere with the formation of the dimer which is created using the IMAGE facility of CHARMM by rotation of 180° about X. As a result the monomers were constrained along the Z axis using CHARMMs MMFP facility in order to maintain proper intermolecular alignment defined by the six intermolecular hydrogen bonds. The van der Waals and electrostatic nonbonded interactions were calculated on the basis of a group-based pair list. The interactions were smoothly truncated at a distance of 10 Å using a 2 Å switching function. A dielectric constant of 1.0 was used.

Once the structure was modified, acceptance of an attempted move was controlled by both the temperature and the difference in the penalty before and after the attempted move. A move which caused a decrease in the penalty was always accepted. A move which increased the penalty was only accepted if a random number between 0 and 1 was less than $\exp(-\Delta\text{penalty}/T)$. This simulated-annealing refinement procedure was controlled by T, the temperature, and an annealing schedule (the rate at which the temperature was lowered during the course of the refinement). The focus of this refinement strategy was to introduce minor structural modifications to the initial structure. Large changes led to conformational space that had already been shown to be excluded through the development of the initial structure. Therefore, the initial value of the temperature was set at 300 so that large structural changes were not possible. At the beginning of the refinement, an equilibration period of 5000 attempted modifications with constant temperature was used. During this period modest structural changes occurred as the defined conformational space was searched. Then the system configuration underwent 2000 attempted modifications or 200 accepted modifications, whichever was first, before the temperature was lowered by 1%. The refinement was terminated when either no successful structural modifications were found at a particular temperature after the 2000 attempted modifications, or after 500 temperature steps. After equilibration, the temperature dropped relatively fast as many of the initial moves were accepted. As the refinement continues, the temperature dropped less often as fewer accepted moves were found.

The global refinement was performed using the program TORC (total refinement of constraints) developed for this study and incorporated into CHARMM as a procedure/subroutine to the CHARMM energy. The program was run on a Silicon Graphics 4 × R800 Power Challenge. Visualization of the the structures was performed on a Silicon Graphics Indigo2 Extreme using InsightII from MSI, Inc.

Accession numbers

The coordinates have been deposited in the Protein Data Bank with accession code 1mag.

Acknowledgements

The authors wish to thank and congratulate the many students and postdocs both past and present in TAC's laboratory who have worked toward this first high-resolution structure of a polypeptide or protein by solid-state NMR. BR is supported by a grant from the Canadian Medical Research Council. TAC gratefully acknowledges support from the National Institutes of Health (R01 AI-23007) and the work was largely performed at the National High Magnetic Field Laboratory supported by NSF Cooperative Agreement DMR-9527035 and the State of Florida.

References

1. Mackerell, A.D., Jr., *et al*., & Karplus, M. (1992). Self-consistent parameterization of biomolecules for molecular modeling and condensed phase simulations. *Biophys. J.* **61,** A 143.
2. Langs, D.A. (1988). Three-dimensional structure at 0.86 Å of the uncomplexed form of the transmembrane ion channel peptide gramicidin A. *Science* **241**, 188–191.
3. Langs, D.A., Smith, G.D., Courseille, C., Precigoux, G. & Hospital, M. (1991). Monoclinic uncomplexed double-stranded, antiparallel, left-handed beta 5.6-helix structure of gramicidin A. *Proc. Natl. Acad. Sci. USA* **88**, 5345–5349.
4. Wallace, B.A. & Ravikumar, K. (1988). The gramicidin pore: crystal structure of a cesium complex. *Science* **241**, 182–187.
5. Pascal, S.M. & Cross, T.A. (1992). Structure of an isolated gramicidin A double helical species by high resolution nuclear magnetic resonance. *J. Mol. Biol.* **226**, 1101–1109.
6. Pascal, S.M. & Cross, T.A. (1993). High-resolution structure and dynamic implications for a double-helical gramicidin A conformer. *J. Biomol. NMR* **3**, 495–513.
7. Bystrov, V.F., Arseniev, A.S., Barsukov, I.L. & Lomize, A.L. (1987). 2D NMR of single and double stranded helices of gramicidin A in micelles and solutions. *Bull. Magn. Reson.* **8**, 84–94.
8. Arseniev, A.S., Bystrov, V.F., Ivnov, V.T. & Ovchinnikov, Y.A. (1984). NMR solution conformation of gramicidin A double helix. *FEBS Lett.* **165**, 51–56.
9. Lomize, A.L., Orekhov, V. & Arseniev, A.S. (1992). Refinement of the spatial structure of the gramicidin A ion channel. *Bioorg. Khim.* **18**,182–200.

10. Cross, T.A. (1994). Structural biology of peptides and proteins in synthetic membrane environments by solid-state NMR spectroscopy. *Annu. Rep. NMR Spectroscopy* **29**, 124–158.
11. Cross, T.A. & Opella, S.J. (1994). Solid-state NMR structural studies of peptides and proteins in membranes. *Curr. Opin. Struct. Biol.* **4**, 574–581.
12. Separovic, F., Pax, R. & Cornell, B.A. (1993). NMR order parameter analysis of a peptide plane aligned in a lyotropic liquid crystal. *Mol. Phys.* **78**,357–369.
13. Koeppe, II R.E., Killian, J.A., Greathouse, D.V. (1994). Orientation of the tryptophan 9 and 11 side chains of the gramicidin channel based on deuterium nuclear magnetic resonance spectroscopy. *Biophys. J.* **66**, 14–24.
14. Hing, A.W. & Schaefer, J. (1993). Rotational-echo double resonance of Val1-[1-^{13}C]Gly2-[^{15}N]Ala3-gramicidin A in multilamellar dimyristoylphosphatidylcholine dispersions. *Biochemistry* **32**, 7593–7604.
15. Prosser, R.S., Davis, J.H., Dahlquist, F.W. & Lindorfer, M.A. (1991). ^{2}H nuclear magnetic resonance of the gramicidin A backbone in a phospholipid bilayer. *Biochemistry* **30**, 4687–4696.
16. Ketchem, R.R., Hu, W. & Cross, T.A. (1993). High-resolution conformation of gramicidin A in a lipid-bilayer by solid-state NMR. *Science* **261**, 1457–1460.
17. Ketchem, R.R., Roux, B. & Cross, T.A. (1966). Computational refinement through solid state NMR and energy constraints of a membrane bound polypeptide. In *Biological Membranes: a Molecular Perspective From Computation and Experiment.* (Merz, K.M., Jr. & Roux, B., eds), pp. 299–322, Birkhauser, Boston, USA.
18. Jordan, P.C. (1990). Ion-water and ion-polypeptide correlations in a gramicidin-like channel: a molecular dynamics study. *Biophys. J.* **58**, 1133–1156.
19. Roux, B. & Karplus, M. (1993). Ion transport in the gramicidin channel: free energy of the solvated right-handed dimer in a model membrane. *J. Am. Chem. Soc.* **115**, 3250–3260.
20. Roux, B. & Karplus, M. (1994). Molecular dynamics simulations of the gramicidin channel. *Annu. Rev. Biomol. Struct. Dyn.* **23**, 731–761.
21. Mackay, D.H., Berens, P.H., Wilson, K.R. & Hagler, A.T. (1984). Structure and dynamics of ion transport through gramicidin A. *Biophys. J.* **56**, 229–248.
22. Elber, R., Chen, D.P., Rojewska, D. & Eisenberg, R. (1995). Sodium in gramicidin: an example of a permion. *Biophys. J.* **68**, 906–924.
23. Chiu, S.-W., Subramanian, S., Jakobsson, E. & McCammon, J.A. (1989). Water and polypeptide conformations in the gramicidin channel: a molecular dynamics study. *Biophys. J.* **56**, 253–261.
24. Woolf, T.B. & Roux, B. (1994). Molecular dynamics simulation of the gramicidin channel in a phospholipid bilayer. *Proc. Natl. Acad. Sci. USA* **91**, 11631–11635.
25. Woolf, T.B. & Roux, B. (1996). Structure, energetics and dynamics of lipid–protein interactions: a molecular dynamics study of the gramicidin A channel in a dmpc bilayer. *Proteins* **24**, 92.
26. Anderson, O.S. & Koeppe, R.E., II (1992). Molecular determinants of channel function. *Physiol. Rev.* **72**, S89–S158.
27. Daumas, P., *et al.*, Pullman, A. (1991). How can the aromatic sidechains modulate the conductance of the gramicidin channel? A new approach using non-coded amino acids. *Int. J. Pept. Protein Res.* **38**, 218–228.
28. Busath, D.D. (1993). The use of physical methods in determining gramicidin channel structure and function. *Annu. Rev. Physiol.* **55**, 473–501.
29. Becker, M.D., Greathouse, D.V., Koeppe, R.E., II. & Andersen, O.S. (1991). Amino acid sequence modulation of gramicidin channel function: effects of tryptophan-to-phenylalanine substitutions on single-channel conductance and duration. *Biochemistry* **30**, 8830–8839.
30. Heitz, F., Gavach, C., Spach, G. & Trudelle, Y. (1986). Analysis of the ion transfer through the channel of 9, 11, 13, 15-phenylalanine gramicidin A. *Biophys. Chem.* **24**, 143–148.
31. Oiki, S., Koeppe, R.E., II. & Andersen, O.S. (1995). Voltage-dependent gating of an asymmetric gramicidin channel. *Proc. Natl. Acad. Sci. USA* **92**, 2121–2125.
32. Gullion, T. & Schaefer, J. (1989). Rotational-echo double-resonance NMR. *J. Magn. Reson.* **81**, 196–200.
33. Garbow, J.R. & McWherter, C.A. (1993). Determination of the molecular conformation of melanostatin using ^{13}C, ^{15}N- REDOR NMR spectroscopy. *J. Am. Chem. Soc.* **115**, 238–244.
34. Smith, S.O. (1993). Magic angle sinning NMR methods for internuclear distance measurements. *Curr. Opin. Struct. Biol.* **3**, 755–759.
35. Raleigh, D.P., Levitt, M.H. & Griffin, R.G. (1988). Rotational resonance in solid-state NMR. *Chem. Phys. Lett.* **146**, 71–76.
36. Ketchem, R.R., Lee, K.-C., Huo, S. & Cross, T.A. (1996). Macromolecular structural elucidation with solid-state NMR-derived orientational constraints. *J. Biomol. NMR* **8**, 1–14.
37. Quine, J.R., Brenneman, M. & Cross, T.A. (1997). Protein structural analysis from solid-state NMR derived orientational constraints. *Biophys. J.* **72**, 2342–2348.
38. Teng, Q., Nichoson, L.K. & Cross, T.A. (1991). Experimental determination of torsion angles in the polypeptide backbone of the gramicidin A channel by solid-state nuclear magnetic resonance. *J. Mol. Biol.* **218**, 607–619.
39. Lee, K.-C., Huo, S. & Cross, T.A. (1995). Lipid–peptide interface: valine conformation and dynamics in the gramicidin channel. *Biochemistry* **34**, 857–867.
40. Hu, W., Lazo, N.D. & Cross, T.A. (1995). Tryptophan dynamics and structural refinement in a lipid bilayer environment: solid-state NMR of the gramicidin channel. *Biochemistry* **34**, 14138–14146.
41. Hu, W. & Cross, T.A. (1995). Tryptophan hydrogen bonding and electric dipole moments: functional roles in gramicidin channel and implications for membrane proteins. *Biochemistry* **34**, 14147–14155.
42. Maruyama, T. & Takeuchi, H. (1997). Water accessibility to the tryptophan indole N–H sites of gramicidin A transmembrane channel: detection of positional shifts of tryptophan 11 and 13 along the channel axis upon cation binding. *Biochemistry* **36**, 10993–11001.
43. Nishikawa, K., Ooi, T., Isogai, Y. & Saito, N. (1972). Tertiary structure of proteins. I. Representation and computation of the conformations. *J. Phys. Soc. Jpn.* **32**, 1331–1337.
44. Akke, M., Forsen, S. & Chazin, W.J. (1995). Solution structure of $(Cd^{2+})_1$-calbindin D_{9k} reveals details of the stepwise structural changes along the apo $\rightarrow(Ca^{2+})^{II}_1 \rightarrow(Ca^{2+})^{I,II}_2$ binding pathway. *J. Mol. Biol.* **252**, 102–121.
45. Cross, T.A., *et al.*, Huo, S. (1994). High-resolution polypeptide structure and dynamics in anisotropic environments: the gramicidin channel. In *Stable Isotope Applications in Biomolecular Structure and Mechanisms.* (Trewhella, J., Cross, T.A. & Unkefer, C.J., eds), pp. 59–71, Los Alamos National Lab, Los Alamos.
46. Metropolis, N., Rosenbluth, A.W., Rosenbluth, M.N., Teller, A.H. & Teller, E. (1953). Equation of state calculations by fast computing machines. *J. Phys. Chem.* **21**, 1087–1092.
47. Kirkpatrick, S., Gelatt, C.D., Jr. & Vecchi, M.P. (1983). Optimization by simulated annealing. *Science* **220**, 671–680.
48. Laskowski, R.A., MacArthur, M.W., Moss, D.S. & Thornton, J.M. (1993). PROCHECK: a program to check the stereochemical quality of protein structures. *J. Appl. Cryst.* **26**, 283–291.
49. Engh, R.A. & Huber, R. (1991). Accurate bond and angle parameters for X-ray protein structure refinement. *Acta Cryst. A* **47**, 392–400.
50. Urry, D.W. (1971). The gramicidin A transmembrane channel: a proposed $\pi_{(L,D)}$ helix. *Proc. Natl. Acad. Sci. USA* **68**, 672–676.
51. Iwata, S., Ostermeier, C., Ludwig, B. & Michel, H. (1995). Structure at 2.8 Å resolution of cytochrome *c* oxidase from *Paracoccus denitrificans*. *Nature* **376**, 660–669.
52. Akiba, T., *et al.*, & Matsubara, H. (1996). Three-dimensional structure of bovine cytochrome *bc* complex by electron cryomicroscopy and helical image reconstruction. *Nat. Struct. Biol.* **3**, 553–561.
53. Kuhlbrandt, W., Wang, D.N. & Fujiyoshi, Y. (1994). Atomic model of plant light-harvesting complex by electron crystallography. *Nature* **367**, 614–621.
54. Pebay-Peyroula, E., Rummel, G., Rosenbusch, J.P. & Landau, E.M. (1997). X-ray structure of bacteriorhodopsin at 2.5 angstroms from microcrystals grown in lipidic cubic phases. *Science* **277**, 1676–1681.
55. Mai, W., Hu, W., Wang, C. & Cross, T.A. (1993). Orientational constraints as three-dimensional structural constraints from chemical shift anisotropy: the polypeptide backbone of gramicidin A in a lipid bilayer. *Protein Sci.* **2**, 532–542.
56. Cross, T.A., Ketchem, R.R., Hu, W., Lee, K.-C., Lazo, N.D. & North, C.L. (1992). Structure and dynamics of a membrane bound polypeptide. *Bull. Magn. Reson.* **14**, 96–101.
57. Lazo, N.D., Hu, W. & Cross, T.A. (1995). Low-temperature solid-state ^{15}N NMR characterization of polypeptide samples for characterization of high definition dynamics by solid-state NMR spectroscopy. *J. Magn. Reson.* **107** B, 43–50.
58. Arumugam, S., *et al.*, & Cross, T.A. (1996). Conformational trapping in a membrane environment: a regulatory mechanism for protein activity? *Proc. Natl. Acad. Sci. USA* **93**, 5872–5876.
59. Cotten, M., Xu, F. & Cross, T.A. (1997). Protein stability and conformational rearrangements in lipid bilayers: linear gramicidin, a model system. *Biophys. J.* **73**, 614–623.

60. Salom, D., Bano, M.C., Braco, L. & Abad, C. (1995). HPLC demonstration that an all Trp to Phe replacement in gramicidin A results in a conformational rearrangement from β-helical monomer to double-stranded dimer in model membranes. *Biochem. Biophys. Res. Commun.* **209**, 466–473.
61. Koeppe, R.E., II., *et al*., & Andersen, O.S. (1992). On the helix sense of gramicidin A single channels. *Proteins* **12**, 49–62.
62. Roux, B. & Karplus, M. (1991). Ion transport in a gramicidin-like channel: dynamics and mobility. *J. Phys. Chem.* **95**, 4856–4868.
63. Tian, F., Lee, K.-C., Hu, W. & Cross, T.A. (1996). Monovalent cation transport: lack of structural deformation upon cation binding. *Biochemistry* **35**, 11959–11966.
64. Hotchkiss, R.D. (1944). Gramicidin, tyrocidine and tyrothricin. *Adv. Enzymol.* **4**, 111–119.
65. Harold, F.M. & Baarda, J.R. (1967). Gramicidin, valinomycin and cation permeability of *Streptococcus faecalis*. *J. Bact.* **94**, 53–60.
66. Jordan, P.C. (1987). Microscopic approaches to ion transport through transmembrane channels: the model system gramicidin. *J. Phys. Chem.* **91**, 6582–6591.
67. Roux, B. & Karplus, M. (1991). Ion transport in a model gramicidin channel: structure and thermodynamics *Biophys. J.* **59**, 961–981.
68. Roux, B. & Karplus, M. (1988). The normal modes of the gramicidin A dimer channel. *Biophys. J.* **53**, 297–309.
69. Turano, B., Pear, M. & Busath, D. (1992). Gramicidin channel selectivity: molecular mechanics calculations for formamidinium, guanidinium and acetamidinium. *Biophys. J.* **63**, 152–161.
70. Smith, R., Thomas, D.E., Atkins, A.R., Separovic, F. & Cornell, B.A. (1990). Solid-state ^{13}C-NMR studies of the effects of sodium ions on the gramicidin ion channel. *Biochim. Biophys. Acta* **1026**, 161–166.
71. Olah, G.A., Huang, H.W., Liu, W. & Wu, Y. (1991). Location of ion-binding sites in the gramicidin channel by X-ray diffraction. *J. Mol. Biol.* **218**, 847–858.
72. Woolf, T.B. & Roux, B. (1997). The binding site in the gramicidin A channel: comparison of molecular dynamics with solid-state NMR data. *Biophys. J.* **72**, 1930–1945.
73. Huo, S., Arumugam, S. & Cross, T.A. (1996). Hydrogen exchange in the lipid bilayer-bound gramicidin channel. *Biophys. J.* **7**, 177–183.
74. Ketchem, R.R., Hu, W., Tian, F. & Cross, T.A. (1994). Structure and dynamics from solid state NMR spectroscopy. *Structure* **2**, 699–701.
75. North, C.L. & Cross, T.A. (1995). Correlations between function and dynamics: time scale coincidence for ion translocation and molecular dynamics in the gramicidin channel backbone. *Biochemistry* **34**, 5883–5895.
76. Becker, M.D., Koeppe, R.E., II & Andersen, O.S. (1992). Amino acid substitutions and ion channel function: model-dependent conclusions. *Biophys. J.* **62**, 25–27.
77. Brooks, B.R., Bruccoleri, R.E., Olafson, B.D., States, D.J., Swaminathan, S. & Karplus, M. (1983). CHARMM: a program for macromolecular energy, minimization and dynamics calculations. *J. Comput. Chem.* **4**, 187–217.
78. Peticolas, W.L. & Kurtz, B. (1980). Transformation of the ϕ-ψ plot for proteins to a new representation with local helicity and peptide torsion angles as variables. *Biopolymers* **19**, 1153–1166.
79. Tejero, R., Bassolino-Klimas, D., Bruccoleri, R.E. & Montelione, G.T. (1996). Simulated annealing with restrained molecular dynamics using CONGEN: energy refinement of the NMR solution structures of epidermal and type-α transforming growth factors. *Protein Sci.* **5**, 578–592.
80. Wang, C., Teng, Q. & Cross, T.A. (1992). Solid-state ^{13}C NMR spectroscopy of a ^{13}C carbonyl-labeled polypeptide. *Biophys. J.* **61**, 1550–1556.
81. Case, D.A. & Wright, P.E. (1993). Determination of high-resolution NMR structures of proteins. In *NMR of Proteins.* (Clore, G.M. & Gronenborn, A.M., eds), pp. 53–91, CRC Press, Boca Raton, USA.
82. Logan, T.M., Zhou, M-M., Nettesheim, D.G., Meadows, R.P., Van Etten, R.L. & Fesik, S.W. (1994). Solution structure of a low molecular weight protein tyrosine phosphatase. *Biochemistry* **33**, 11087–11096.
83. Jeffrey, G.A. & Saenger, W. (1994). *Hydrogen Bonding in Biological Systems.* Springer-Verlag, Berlin, Germany.